ACS APPLIED MATERIALS & INTERFACES

Research Article

www.acsami.org

Mussel-Inspired Artificial Grafts for Functional Ligament Reconstruction

Hong Li,[†] Shiyi Chen,*[,†] Jiwu Chen,[†] Jiang Chang,[‡] Mengchi Xu,[‡] Yaying Sun,[†] and Chengtie Wu*[,‡]

[†]Department of Sports Medicine, Huashan Hospital, Fudan University, 12 Wulumuqi Zhong Road, Shanghai 200040, People's Republic of China

[‡]State Key Laboratory of High Performance Ceramics and Superfine Microstructure, Shanghai Institute of Ceramics, Chinese Academy of Sciences, 1295 Dingxi Road, Shanghai 200050, People's Republic of China

ABSTRACT: The development of an artificial graft with distinct osteogenetic activity to enhance osseointegration and to induce the formation of biomimetic tissue structure for ligament reconstruction remains a significant challenge. Inspired by mussels, biomimetic calcium phosphate apatite/polydopamine hybridized−polyethylene terephthalate (APA/PDA−PET) grafts were successfully prepared. The efficacy and mechanism of APA/PDA−PET grafts to induce osseointegration were systematically investigated. The results from the *in vitro* study indicated that the prepared APA/PDA−PET grafts support the attachment of bone marrow stromal cells (BMSCs) and stimulate the proliferation and osteogenic/angiogenic differentiation of BMSCs via activation of the PKC/p-ERK1/2 signaling pathway. *In vivo*, histological and radiological results further demonstrate that the APA/PDA−PET grafts significantly improve osseointegration by inducing the formation of new bone tissue and the fibrocartilage transitional zone compared with pure PET grafts. In addition, the pull-out strength of the APA/PDA−PET grafts is significantly higher than that of the pure PET grafts 12 weeks after surgery. These results suggest that this mussel-inspired biomimetic method is an effective strategy for modifying artificial grafts, and the prepared APA/PDA−PET grafts, which possess a beneficial interface, can significantly improve *in vivo* osseointegration for ligament reconstruction via the synergistic effect of polydopamine and apatite.

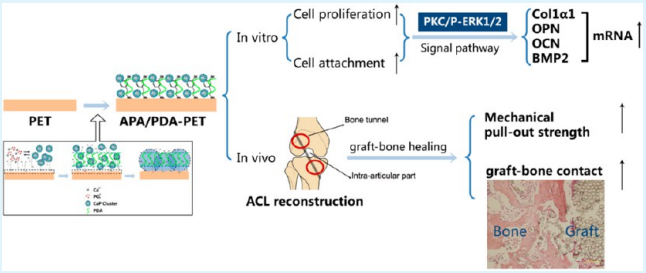

KEYWORDS: *mussel, artificial ligament, apatite, polydopamine, osseointegration*

1. INTRODUCTION

Ligament rupture commonly occurs during sports activities, and operative reconstruction of the injured ligament is required.[1−3] To avoid complications induced by autograft or allograft tendons (e.g., donor site morbidity and disease transmission), artificial ligament grafts are the accepted choice for ligament reconstruction in the human body.[4−6] Because of their typically nondegradable and mechanically strong properties, the artificial ligament grafts promise a fast recovery and quick return to sports after the operation compared to autograft or allograft tendon grafts.[7] Although most of the available artificial ligaments possess some of the beneficial properties of native ligaments, the formation of biomimetic tissue structures remains challenging to induce at the native ligament−bone interface, and poor graft−bone healing with a fibrous scar tissue band is always observed at the graft−bone interface.[8,9] The direct insertion sites of the native anterior cruciate ligament (ACL) on the tibia and femur are composed of four zones: ligament, unmineralized fibrocartilage, mineralized fibrocartilage and bone tissues.[10] This highly specialized fibrocartilage structure provides an effective transfer of the mechanical load from the graft to the bone. Poor graft−bone integration cannot bear the stress from ligament motion during sports activity, which results in graft failure. The preparation of an artificial graft with distinct osteogenetic activity that enhances osseointegration and induces biomimetic tissue structure for ACL reconstruction after implantation in the bone tunnel remains a significant challenge.

Bone-like calcium phosphate (CaP) apatite has been widely used as a bioactive biomaterial for the regeneration of bone tissue due to its ability to induce protein adsorption, cell adhesion and osteoblastic differentiation in progenitor cells.[10−12] CaP has been an effective material for inducing the formation of an insertion-like tissue at the tendon−bone interface. In a rabbit ACL reconstruction experiment, CaP particles were implanted at the tendon−bone interface, and a classic and direct connection composed of four zones (e.g., tendon, fibrocartilage, calcified cartilage and new bone basal plate) was observed there.[10] Mutsuzaki et al.[11] prepared CaP-hybridized tendon grafts using an alternate soaking process, and they observed that the grafts reduced bone tunnel enlargement, and the gap area was associated with an insertion-like formation at the interface during ACL reconstruction in a goat model. Recently, Zhao et al.[12] applied CaP bioceramic particles to regenerate the tendon−bone interface and demonstrated that the interposition of CaP

Received: March 17, 2015
Accepted: June 22, 2015
Published: June 22, 2015

DOI: 10.1021/acsami.5b05109
ACS Appl. Mater. Interfaces 2015, 7, 14708−14719

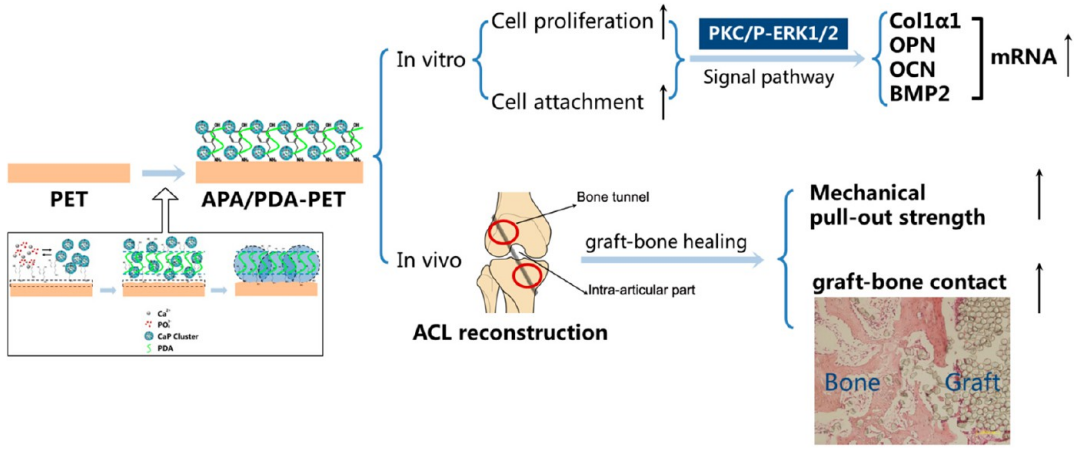

Figure 1. Schematic illustration for mussel-inspired apatite/polydopamine hybridized−polyethylene terephthalate (APA/PDA−PET) grafts stimulating *in vitro* osteogenic/angiogenic differentiation for BMSCs via activating P-ERK signaling pathway and enhancing *in vivo* osseointegration for anterior cruciate ligament (ACL) reconstruction. PET, polyethylene terephthalate; PDA, polydopamine; APA, apatite.

particles enhanced tendon−bone healing associated with the formation of fibrocartilage at the tendon−bone interface. Previous studies suggested that CaP apatite is beneficial for reconstructing the interface between the tendon and bone. However, few studies using CaP apatite on a PET artificial ligament have been reported. Because the artificial ligament also has poor osseointegration with the bone tunnel, which is similar to the tendon graft, we assumed that CaP apatite might be useful for modifying the artificial ligament to improve its osteogenic activity. Previously, we prepared polyethylene terephthalate (PET) artificial grafts modified with hydroxyapatite particles using a solution-soaking method to enhance their osseointegration.[13] However, this method does not lead to a homogeneous apatite coating on the surface of the PET grafts despite their improved bioactivity, limiting their further application.

Inspired by the adhesive proteins in mussels, Lee et al.[14] prepared a polydopamine (PDA) film with a numerous catechol moieties, OH^- and NH_2^- on different material surfaces. PDA can form strong covalent and noncovalent interactions with substrates.[15] PDA is a polymer formed by the polymerization of dopamine, which occurs in a manner reminiscent of melanin formation and involves the oxidation of catechol to a quinone, and reacts with amines and other catechols/quinones to form an adherent polymer. In this process, an alkaline Tris−HCl solution accelerates the oxidation of catechol to quinine followed by polymerization in a manner analogous to melanin formation. Because of these bioactive groups (e.g., OH^- and NH_2^-), PDA improved CaP apatite mineralization in a simulated body fluid (SBF).[15−17] The results from our recent study indicated that polydopamine-modified bioceramic scaffolds can enhance the attachment, proliferation and osteogenic differentiation of osteoblast-like cells.[15,18] Inspired by the distinct advantages of CaP apatite (APA) and polydopamine, the preparation of mussel-inspired artificial ligaments with APA/PDA hybrid layers would be beneficial for improving osseointegration and might induce the formation of a biomimetic tissue structure for reconstructing ACL. Therefore, the aim of this study was to prepare mussel-inspired APA/PDA−PET ligament grafts using a polydopamine-involved biomimetic method and to systematically investigate the *in vitro* osteogenic differentiation and mechanism for bone marrow stromal cell (BMSC) response to APA/PDA−PET grafts, *in vitro* ligamentization potential for fibroblast response to PDA−PET grafts and *in vivo* osseointegration for ACL reconstruction (as shown in Figure 1).

2. MATERIALS AND METHODS

2.1. Preparation and Characterization of Mussel-Inspired APA/PDA−PET Grafts. To prepare apatite/polydopamine hybrid layer-modified PET (named APA/PDA−PET) grafts, 2 types of Ca, P containing-simulated body fluids (2SBF) were prepared, and the pH was adjusted to 8.0 using tris(hydroxymethyl)aminomethane (Tris). Then, dopamine hydrochloride was dissolved in 2SBF at a concentration of 2 mg/mL under stirring. The PET grafts (5 × 5 cm) were soaked in the dopamine/2SBF solution for 72 h at room temperature. After soaking, the grafts were rinsed in water and dried under N_2 gas to yield the APA/PDA−PET grafts. The polydopamine-modified PET (PDA−PET) grafts were prepared using a similar method with a Tris-HCl/dopamine solution. The APA/PDA−PET grafts, PDA−PET and pure PET grafts were used to investigate the *in vitro* osteogenic differentiation and mechanism for BMSC response to APA/PDA−PET grafts and *in vivo* osseointegration for ACL reconstruction. The PDA−PET and pure PET grafts were used to investigate the *in vitro* ligamentization potential for fibroblast response to the PDA−PET grafts.

The surface morphology and surface composition of the prepared grafts were characterized by scanning electron microscopy (SEM, S-4800, Hitachi, Japan) and energy dispersive spectrometry (EDS, Magellan 400, FEI company, USA). Small pieces of the samples were vacuum coated with gold, placed in the vacuum chamber of the SEM and viewed at a 1 kV accelerating voltage. The contact angle of deionized water on various grafts was measured in air using a contact angle meter (DSA100 Kruss, Germany). The scaffolds were cut into rectangular sections (5 × 2 × 0.2 cm) and kept flat on a plane solid support, maintained at 20 °C. Drop orientation was determined using the sessile drop method. The liquid droplet volume was 5.0 ± 0.5 μL and images of droplets were seized after every 30 s, using a camera. The liquid was dropped on different corners of each sample. The average contact angle was calculated from six independent measurements at random sites on each graft.

2.2. Isolation and Culture of Bone Marrow Stromal Cells (BMSCs) on APA/PDA−PET Grafts. *2.2.1. Cell Seeding on Grafts.* Rabbit BMSCs were isolated from the femur bones of rabbits (1 month old) and cultured in Dulbecco's modified Eagle's medium, (DMEM HyClone, China) supplemented with 10% fetal calf serum (Invitrogen) and 1× penicillin−streptomycin (Invitrogen). The cells were cultured at 37 °C in a 5% CO_2 incubator, and the medium was changed every other day. The APA/PDA−PET, PDA−PET and pure PET sheets were cut into discs with a diameter of 10 mm to cover the bottom of 24-well plates. BMSCs were seeded on each sample using 3.5 × 10^5 cells.

DOI: 10.1021/acsami.5b05109
ACS Appl. Mater. Interfaces 2015, 7, 14708−14719

2.2.2. Cell Proliferation and Cell Cycle analysis. Cell proliferation (n = 5) was assessed using a CCK-8 proliferation assay. After the cells were cultured for 1, 3, 5 and 7 days, 10 μL of the CCK-8 solution (Dojindo Molecular Tech. Inc., China) was added to each well. After the plate was incubated at 37 °C for an additional 4 h, the optical density (OD) at 450 nm was measured against a blank solution using a microplate reader (MultiSkan FC, Thermo).

For cell cycle analysis (n = 3), the cells were treated for 3, 5 and 7 days. The cells were harvested, fixed with cold 70% ethanol for 30 min at 4 °C and then incubated in the dark with RNase (100 mg/mL) and propidium iodide (50 mg/mL) for 30 min at 37 °C. A total of 5000 cells were examined by flow cytometry using a Canto I flow cytometer (Becton-Dickinson, Franklin Lakes, NJ).

2.2.3. Scanning Electron Microscopy (SEM). For the morphological observation, the samples (n = 3) were washed twice with phosphate buffered saline (PBS) and immersed in PBS containing 1.25% glutaraldehyde for 2 h. The fixative was removed by washing with 0.1 M PBS and postfixed in 1% osmic acid (4 °C) for 2 h. Then, the samples were dehydrated in a graduated ethanol series (30, 50, 70, 90 and 100%). The samples were gold sputtered under vacuum and examined using SEM (S-4800, Hitachi, Japan).

2.2.4. Real Time-Polymerase Chain Reaction (RT-PCR) Analysis. The expression levels of the bone-related genes were compared between the groups. For each culturing period, the total RNA was extracted with the TRIzol reagent (Invitrogen) based on the manufacturer's protocol. Isolated RNA was reversely transcribed using Reverse Transcriptase M-MLV (Takara) and then amplified using Takara SYBR Premix Ex Taq (Takara) according to the manufacturer's instructions followed by PCR using the primers listed in Table 1. The gene expressions were normalized to that of β-actin in all of the samples (n = 3). Three parallel replicates were evaluated for each sample.

Table 1. Primer Sequences

gene	sequences
β-actin	forward: GCATGGGCCAGAAGGACTCGTA
	reverse: TCGCGGTTGGCCTTGGGGTTCA
ALP	forward: CGGTGGTGCTGGCGGTGGAC
	reverse: GCGGCCTCGTGCGTGCTCTC
osteopontin	forward: GTGGACAGCGAGGACTTGGATG
	reverse: GGCCTCGCGCTTATATTGTCTGG
Runx2	forward: CCCCGGGAACCCAGAAGGCACAGA
	reverse: CATAGGACCACGGCGGGGAAGACT
VEGF	forward: AGCCTTCCTGCGTGCCTCTGGT
	reverse: TCTTTGGTCTGCATTCACATTTG

2.2.5. Western Blot analysis. After culturing, the cells were harvested and lysed with cell lysis buffer. Then, the protein concentrations were measured using the BCA protein assay kit (Pierce Biotechnology Inc., USA). The proteins were run on SDS-PAGE gels and electrotransferred to a nitrocellulose membrane at 4 °C for 2 h. The blots were probed with BMP-2 (1:200, Santa Cruz Biotechnology, Inc., USA), HIF-1α (1:500, Santa Cruz Biotechnology, Inc., USA) and VEGF antibody (1:400, Santa Cruz Biotechnology, Inc., USA) overnight at 4 °C. After reaction with the secondary antibody, the proteins were detected by chemiluminescence according to the manufacturer's recommendations (ECL Western Blotting Substrate Pierce Biotechnology Inc., USA) and detected on X-ray film. β-actin antibody (1:1000, Santa Cruz Biotechnology, Inc., USA) was used as an internal control (n = 3). Three parallel replicates were evaluated for each sample.

To investigate further the possible mechanism of the APA/PDA–PET grafts for the osteogenic/angiogenic differentiation of BMSCs, the cell cultures were treated with protein kinase C (PKC) inhibitor (100 μM) (Santa Cruz Biotechnology, Inc., USA), and the cells were cultured for 5 days. Western blot analysis was performed as described above. The expression levels of the related proteins were detected including Phospho-Erk1/2 (antibody, 1:500, Cell Signaling Technology, Inc., USA), Erk1/2 (antibody, 1:800, Cell Signaling Technology, Inc., USA), BMP-2 (antibody, 1:100, Santa Cruz Biotechnology, Inc., USA), OPN (antibody, 1:400, Santa Cruz Biotechnology, Inc., USA) and OCN (antibody, 1:600, Santa Cruz Biotechnology, Inc., USA).

2.3. Ligamentization Potential of the PDA–PET Grafts. Because PDA is coated onto the intra-articular portion of the PET graft, the PDA–PET and pure PET grafts were used to investigate the *in vitro* ligamentization potential for fibroblast response. To investigate the ligamentization potential of the PDA–PET grafts, rat fibroblasts (The Key Laboratory of Molecular Medicine, Fudan University, China) were cultured on the PDA–PET and PET grafts. The rat fibroblasts were cultured in DMEM (Dulbecco's modified Eagle's medium, HyClone, China) supplemented with 10% fetal calf serum (Invitrogen), 1× penicillin–streptomycin (Invitrogen). The cells were cultured at 37 °C in a 5% CO_2 incubator, and the medium was changed every other day. The PDA–PET and pure PET sheets were cut into discs with a diameter of 10 mm to cover the bottom of 24-well plates. The cells were seeded on each sample using 5×10^5 cells.

For the cell proliferation studies (n = 5), the cell proliferation was assessed using a CCK-8 proliferation assay. After the cells were cultured for 1, 3 and 7 days, 10 μL of the CCK-8 solution (Dojindo Molecular Tech. Inc., China) was added to each well. After the plate was incubated at 37 °C for an additional 4 h, the optical density (OD) at 450 nm was measured against a blank solution using a microplate reader (MultiSkan FC, Thermo). For the RT-PCR analysis (n = 3), the gene expression levels were compared between the groups. At each culturing time period, the total RNA was extracted with the TRIzol reagent (Invitrogen) based on the manufacturer's protocol. Isolated RNA was reversely transcribed using Reverse Transcriptase M-MLV (Takara) and then amplified using Takara SYBR Premix Ex Taq (Takara) according to the manufacturer's instructions followed by PCR using the primers listed in Table 2. The gene expressions were normalized to that of β-actin in all of the samples. For the Western blot analysis (n = 3), the cells were harvested and lysed with lysis buffer. Then, the protein concentrations were measured using the BCA protein assay kit (Pierce Biotechnology Inc., USA). The proteins were run on SDS-PAGE gels and electrotransferred to a nitrocellulose membrane at 4 °C for 2 h. The blots were probed with Collagen I (1:800, Santa Cruz Biotechnology, Inc., USA), Collagen III (1:600, Santa Cruz Biotechnology, Inc., USA) and VEGF antibody (1:200, Santa Cruz Biotechnology, Inc., USA) at various dilutions overnight at 4 °C. After reaction with the secondary antibody, the proteins were detected by chemiluminescence according to the manufacturer's recommendations (ECL Western Blotting Substrate Pierce Biotechnology Inc., USA) and detected on X-ray film. β-Actin antibody (1:800, Santa Cruz Biotechnology, Inc., USA) was used as an internal control. Three parallel replicates were evaluated for each sample.

Table 2. Primer Sequences

gene	sequences
β-actin	forward: CCTAAGGCCAACCGTGAAAAGATG
	reverse: GTCCCGGCCAGCCAGGTCCAG
Collagen I	forward: TCCTGACGCATGGCCAAGAAGACA
	reverse: ACAGCACTCGCCCTCCCGTTTTTG
Collagen III	forward: GGTCCTGCTGGTCCTATTG
	reverse: CTCTCCGGGGGCACCTCTTTCT
VEGF	forward: CCAGGCTGCACCCACGAC
	reverse: AGCCCGCACACCGCATTAG

2.4. Animal Experiments. All of the animal experiments were approved by the Animal Care and Use Committee at our university. The grafts were cut into sheets measuring 5 × 0.9 cm, and these sheets were rolled into a cylindrical graft that was 5 cm in length and 0.3 cm in diameter for *in vivo* implantation. Sixty mature male New Zealand rabbits (6 months old; 20 rabbits in each group) underwent an operative ACL reconstruction procedure. Anesthesia was induced by the intravenous administration of 3% pentobarbital (30 mg/kg). After skin preparation and disinfection, a medial incision was made on the right knee. The native ACL was exposed and removed from the insertion

DOI: 10.1021/acsami.5b05109
ACS Appl. Mater. Interfaces 2015, 7, 14708–14719

sites by sharp dissection. Next, a 3 mm diameter tunnel was drilled in the femoral and tibial insertion sites of the ACL, as shown in Figure 1. The prepared grafts were pulled manually into the bone tunnel. The APA/PDA−PET, PDA−PET and PET grafts were implanted into the right knees of 60 rabbits. The ends of the grafts were sutured with the adjacent periosteum and soft tissue at the bone portal. Then, the wound was closed. The postoperative rabbits were returned to their cages and allowed to move freely. Ten rabbits in each group were sacrificed at 6 and 12 weeks after surgery for the following examinations.

2.5. Microcomputed Tomography (micro-CT) Analysis. The animals were sacrificed at each time point after surgery, and the femoral-*graft*-tibia complex samples (n = 5) were fixed in 10% formalin for 24 h. These samples were collected for micro-CT analysis and magnetic resonance imaging (MRI). All of the bone tunnel model images were acquired using a Siemens Inveon Micro-CT scanner (Siemens Medical Solution, Germany). The acquisition parameters: voltage = 80 kV, current = 500 uA, exposure time = 800 ms, binning = 2, magnification = med (the transaxial and axial FOV were 61.05 and 40.70 mm, respectively). The mineralized tissue was distinguished from non-mineralized tissue using a global thresholding procedure with a value of approximately 1.20 g cm^{-3} (25% lower than 1.6 g cm^{-3}). Here, only the area with a cylinder region (3 mm in diameter and 10 mm in height) in the middle bone tunnel was measured. The bone volume in each defect was recorded as the measurement of new bone regeneration.

2.6. MRI Scan. A 3.0-T MRI scanner (Magnetom Verio, Siemens, Germany) was used to image the femoral-*graft*-tibia complex samples that were in a relaxed extended position. Sagittal and axial images were obtained with oblique proton density−fat saturation: repetition time, 5000 ms; echo time, 25 ms; matrix, 320 × 272; field of view, 100 × 100 mm; slice thickness, 3 mm. The images were imported into the Siemens Software Package (NUMARIS/4, SyngoMR B17, Siemens, Germany) to analyze the graft−bone interface.

2.7. Histological Examinations. After the CT and MRI scans, the femoral-*graft*-tibia samples were fixed in 10% formalin for 48 h. All of the samples were decalcified in 10% EDTA, which was changed twice each week. After 4 weeks, the samples were embedded in paraffin. The samples were sectioned with a thickness of 5 μm perpendicular to the longitudinal axis of the grafts in the middle portion of the bone tunnel. The sections were treated with hematoxylin−eosin (H&E) and masson trichrome staining for histological evaluation. All of the images were visualized using inverted light microscopy (IX71SBF-2, Olympus Co., Japan). The digital images were recorded using a DP Manager (Olympus Optical Co., Japan). Histomorphometric analysis was performed according to a previously reported procedure.[35] Five sections were chosen, and each section was divided into 4 quadrants to determine the graft−bone interface width. In each of the 4 quadrants, the interface width was measured as the distance between the edge of the bone tunnel and the outer graft determined under 200× magnification. Four separate measurements were obtained in each of the quadrants for a total of 16 measurements for each specimen. Then, the average interface width for each specimen was determined by averaging the values obtained from each specimen. In addition, the interface tissue at the graft−bone interface was morphologically graded according to a previously reported method,[10] and these grades included (1) separation between the bone and graft, (2) interface without collagen fiber continuity, (3) collagen fiber continuity (indirect connection) and (4) direct type of insertion. Each group contained ten specimens (i.e., five tibial and five femoral specimens) at each time point. When two types of interface tissues were found in the same section, the specimen was assigned to the higher grade. The two investigators who performed the histomorphometric analysis were blinded to the type of animal treatment.

2.8. Biomechanical Testing. Immediately after sacrifice, the femoral-*graft*-tibia samples (n = 5) were harvested from each knee and prepared for mechanical testing. The pull-out load of the grafts in the bone tunnel was tested using an Instron materials testing system machine (8874, Instron Co. USA). The femoral and tibial bone samples were fixed firmly in clamps. The bone tunnel was oriented parallel to the testing axis. Prior to conducting the tensile test, the specimen was preloaded with a preload of 1 N for 5 min. Immediately after preconditioning, the ultimate pull-out load was investigated using an elongation rate of 2 mm/min. For each specimen, the testing was completed when the graft ruptured or was pulled out of the bone tunnel. The maximal pull-out load (N) was recorded.

2.9. Statistical Analysis. The mean and standard deviation were used to describe the data, and the data analysis was performed using the Stata10.0 software (Stata Corp, USA). The statistical analysis of the quantitative results was carried out using a one way ANOVA test among the groups. The statistical significance level was set to 0.05.

3. RESULTS

3.1. Characterization of Grafts. The optical graphs indicated that the PET grafts were white. The PDA−PET and APA/PDA−PET grafts were brown and black (Figure 2A). SEM

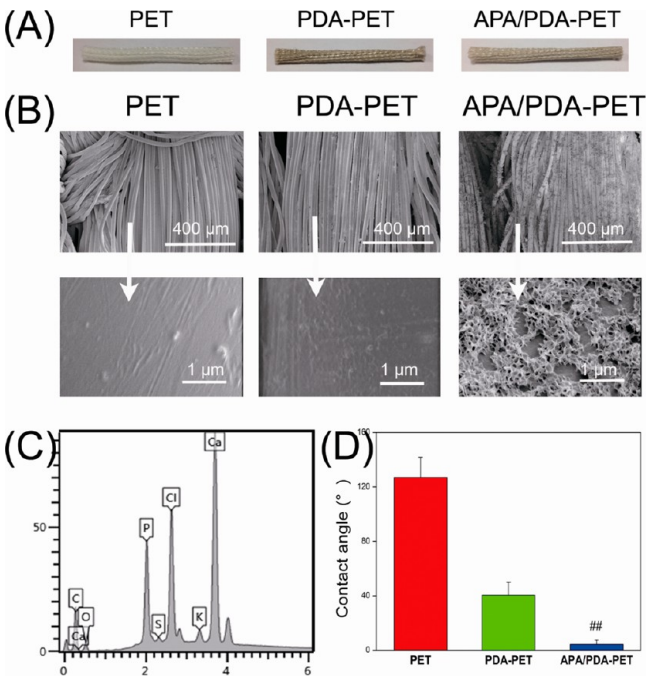

Figure 2. (A) Overview of PET, PDA−PET and APA/PDA−PET grafts. (B) SEM morphology of three grafts. As shown in APA/PDA−PET group, an apatite/polydopamine hybrid nanolayer was formed on the surface of PET. (C) EDS analysis of APA/PDA−PET grafts. Ca and P signals in the pattern were obvious. (D) Water contact angle of three grafts. APA/PDA−PET grafts have significantly increased surface hydrophilicity as compared to [PDA−PET and pure PET grafts. PET, polyethylene terephthalate; PDA, polydopamine; APA, apatite.

analysis (Figure 2B) revealed that the PET grafts had a smooth surface. After mineralization, the PA/PDA hybrid layer, which has a flake morphology, was homogeneously deposited on the surface of the PET grafts, and the particle size was approximately 200 nm. EDS analysis indicated that distinct Ca and P signals were produced by the APA/PDA−PET grafts (Figure 2C). The APA/PDA−PET grafts exhibited a significantly decreased water contact angle compared to that of the PDA−PET and pure PET grafts (Figure 2D).

3.2. Morphology, Proliferation and Bone-Related-Gene/Protein Expression of BMSCs on APA/PDA−PET Grafts. The attachment and morphology of rabbit BMSCs on three groups were examined by SEM (Figure 3). The cells attached well on the three groups and bridged over two fibers of the graft after 1 and 3 days of culture. The CCK-8 test results indicated that the cells on the three groups proliferated as the culture time increased (Figure 4A). The cells in the APA/PDA−PET group exhibited a significantly higher proliferation level

DOI: 10.1021/acsami.5b05109
ACS Appl. Mater. Interfaces 2015, 7, 14708−14719

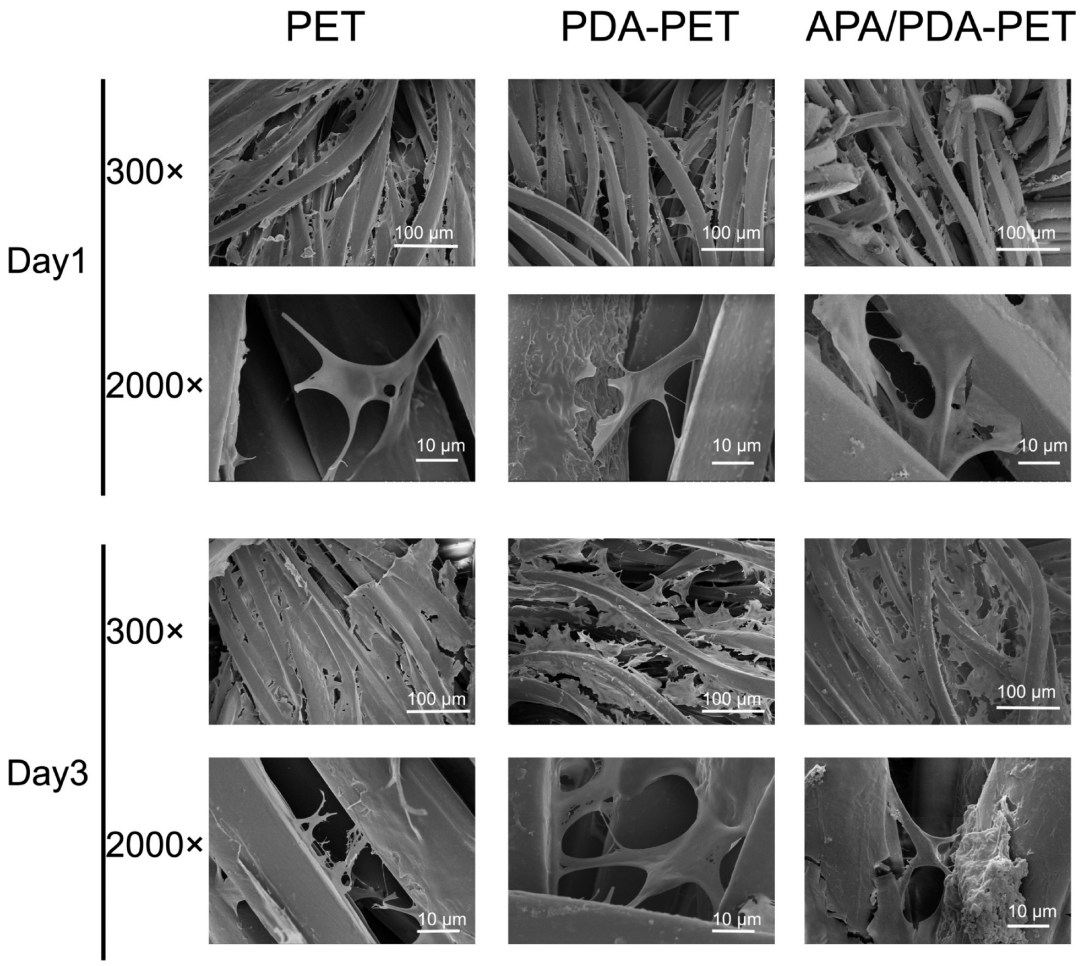

Figure 3. SEM micrographs of BMSCs after cultured on PET, PDA−PET and APA/PDA−PET grafts at day 1 and 3. Cells attach well on the APA/PDA−PET grafts. PET, polyethylene terephthalate; PDA, polydopamine; APA, apatite.

than those in the PDA−PET and PET groups after 7 days of culture ($p < 0.01$). Cell cycle analysis indicated that the APA/PDA coating decreased the number of cells in G1 and increased the number of cells in the S-phase (Figure 5).

The expression levels for alkaline phosphatase (ALP), osteopontin (OPN), runt-related transcription factor 2 (RUNX2) and vascular endothelial growth factor (VEGF) of BMSCs on the APA/PDA−PET grafts were significantly higher than those on the PDA−PET and pure PET grafts after 7 days of culture (Figure 4B).

Western blot analysis demonstrated that the expression of osteogenic factors (bone morphogenetic protein 2 (BMP-2)) on the APA/PDA−PET group was higher than that of the PDA−PET and PET groups at each time point (Figure 4C). The expression of angiogenic factors (VEGF and hypoxia inducible factor-1α (HIF-1α)) of BMSCs was also significantly elevated by the APA/PDA−PET grafts. In addition, the inhibition of PKC activity further inhibited BMP-2, OPN and osteocalcin (OCN) production in the APA/PDA group (Figure 4D). P-ERK1/2 production was substantially reduced after PKC inhibition in the APA/PDA group. For the PET group, no significant reduction in the P-ERK1/2 production was observed after PKC inhibition.

3.3. Proliferation and Ligamentization Related Gene/Protein Expression of Fibroblasts on PDA−PET Grafts. The CCK-8 results (Figure 6A) revealed that the cells proliferated with time on both of the films. At 7 days, the cells in the PDA−PET group exhibited a significantly higher proliferation level than those in the PET groups after 7 days of culture ($p < 0.001$). On the basis of the RT-PCR test, significant differences in the levels of RNA expression were observed between cells that were cultured on the pure PET films and PDA-coated films after 7 days of culture (Figure 6B). The RNA expression levels for Collagen I, Collagen III and VEGF on the PDA−PET group were significantly higher than those for the control group after 7 days of culture. Western blot analysis also indicated that the expression of Collagen I and VEGF on the PDA−PET group was higher than those of the PET groups after 7 days of culture (Figure 6C).

3.4. In Vivo Osseointegration of APA/PDA−PET Grafts. The micro-CT images of the bone tunnels are shown in Figure 7A. The APA/PDA−PET group exhibited better bone regeneration ability than the PDA−PET and PET groups. The bone tunnels implanted with the APA/PDA−PET grafts were filled a much larger quantity of mineralized tissue, and the bone tunnels implanted with pure PET grafts exhibited little mineralized tissue formation around the grafts after 12 weeks of implantation. In addition, the bone tunnel area of the APA/PDA−PET group appeared smaller than that of the PET group in both the femoral and tibial tunnels (Figure 7A). Quantitative analysis of the CT scan indicated that the volume of newly formed mineralized tissue in the femoral tunnel for APA/PDA−PET was much higher than that for PET at both 6 (7.4 ± 2.0 mm^3 vs 2.4 ± 1.5 mm^3; $p = 0.03$) and 12 weeks (9.0 ± 1.4 mm^3 vs 1.3 ± 1.0 mm^3; $p < 0.001$) (Figure 7B). Similarly, the volume of newly

DOI: 10.1021/acsami.5b05109
ACS Appl. Mater. Interfaces 2015, 7, 14708−14719

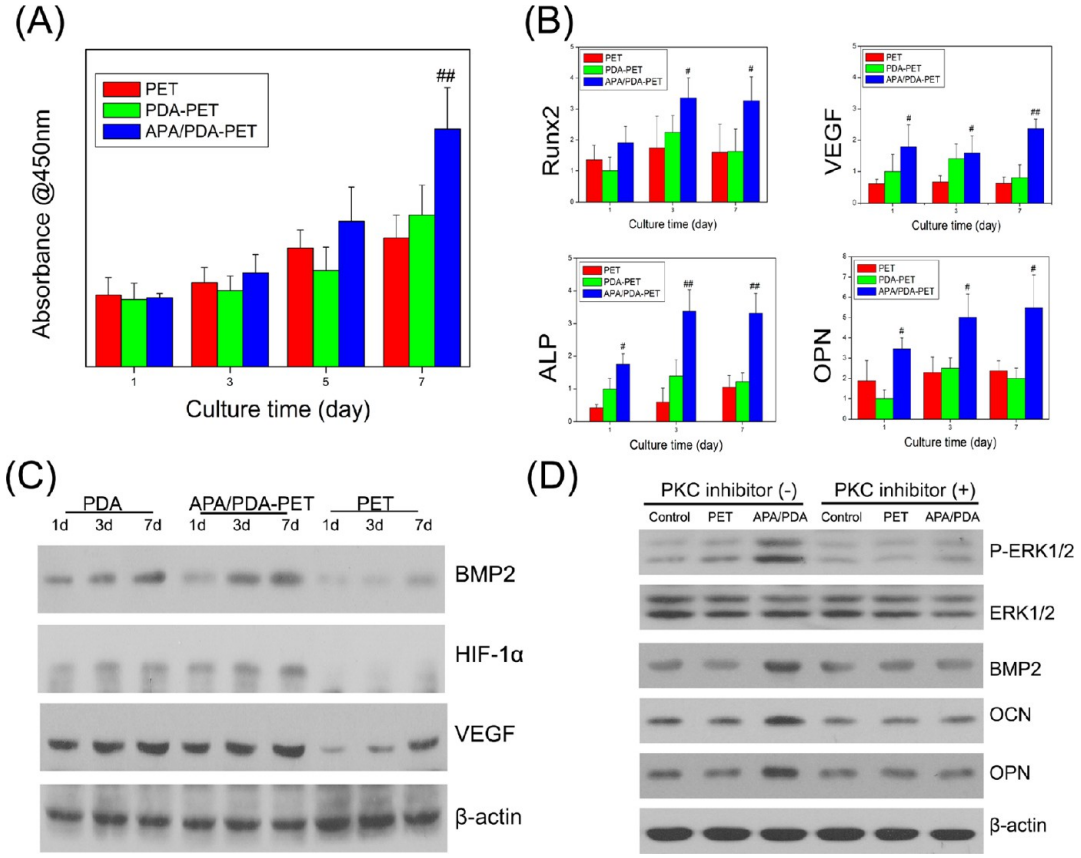

Figure 4. (A) Proliferation of BMSCs on PET, PDA−PET and APA/PDA−PET grafts. (B) Osteogenic/angiogenic gene levels of Runx2, VEGF, ALP and OPN for BMSCs on three grafts. (C) Western blotting analysis for BMP-2, HIF-1α and VEGF proteins. (D) Western blotting analysis for P-ERK1/2 and ERK1/2 signaling pathway and following protein expression BMP-2, OPN and OCN with or without PKC inhibitor. ## ($p < 0.01$) or # ($p < 0.05$) indicate a significant difference between APA/PDA−PET and PET group. APA/PDA−PET grafts significantly enhanced the proliferation and osteogenic/angiogenic gene and protein expression of BMSCs via activating P-ERK1/2 signaling pathway. PET, polyethylene terephthalate; PDA, polydopamine; APA, apatite.

formed mineralized tissue in the tibial tunnel for APA/PDA−PET was also significantly higher than that for PET at both 6 (2.8 ± 1.0 mm^3 vs 0.9 ± 0.3 mm^3; $p = 0.01$) and 12 weeks (6.9 ± 1.5 mm^3 vs 0.5 ± 0.6 mm^3; $p < 0.001$). In addition, the PDA−PET grafts induced more newly formed mineralized tissue than the PET grafts after 12 weeks of implantation (Figure 7B).

The MRI images further revealed the healing quality of the graft−bone region for the three groups 12 weeks after surgery (Figure 7C). All of the images exhibited mild joint effusion. For the PET group, a swelling and diffused hyperintense area was present at the graft−bone interface in the femoral and tibial tunnels. For the PDA−PET group, a low intensity signal band was observed in the femoral tunnel, a partial high intensity signal band was observed in the tibial tunnel. For the APA/PDA−PET group, a low intensity signal band across the bone tunnel at the tendon−bone interface was observed in both the femoral and tibial tunnels (Figure 7C).

For the biomechanical analysis, all of the specimens failed in the pull-out testing from the tibial tunnel, and no graft rupture occurred. The maximal pull-out load of the APA/PDA−PET group was significantly higher than that of the PET group (84.8 ± 10.8 N vs 56.8 ± 6.1 N, $p < 0.01$ at week 6; 104.2 ± 12.8 N vs 61.2 ± 9.1 N, $p < 0.01$ at week 12) (Figure 7D). No significant difference in the maximal pull-out load was detected between the PDA−PET and PET groups at 12 weeks ($p > 0.05$), and the maximal pull-out load of the APA/PDA−PET group was significantly higher than that of the PDA−PET group at 12 weeks ($p = 0.002$).

The histological results are shown in Figure 8. Six weeks after surgery, no significant difference in the graft−bone interface was observed between the APA/PDA−PET and PET groups in the tibial tunnel. In the femoral tunnel, some new bone tissue formation was observed at the graft−bone interface for the APA/PDA−PET group, and the PET group exhibits a lot of fibrous tissue at the graft−bone interface 6 weeks after surgery. The graft−bone interface of the APA/PDA−PET group appeared thinner compared to that of the PET group. Twelve weeks after surgery, the PET group still had a fibrous scar tissue band at the graft−bone interface in both the femoral and the tibial tunnels. In the APA/PDA−PET group, a large amount of new bone tissue at the interface grew onto the graft, and good osseointegration (close bone graft contact) was observed in the femoral tunnel 12 weeks after surgery (Figure 8A). The histomorphometric analysis revealed that the interface width of the APA/PDA−PET group was much smaller than that of the PET group in both the femoral ($p < 0.001$) and tibial ($p < 0.001$) tunnels at 12 weeks (Figure 8D). The interface width of the APA/PDA−PET group was much smaller than that of the PDA−PET group in the tibial tunnel ($p = 0.01$) 12 weeks after implantation. No significant difference in the interface width between the PDA−PET and PET groups was observed in the femoral ($p > 0.05$) and tibial ($p > 0.05$) tunnels at 12 weeks. (Figure 8D).

DOI: 10.1021/acsami.5b05109
ACS Appl. Mater. Interfaces 2015, 7, 14708−14719

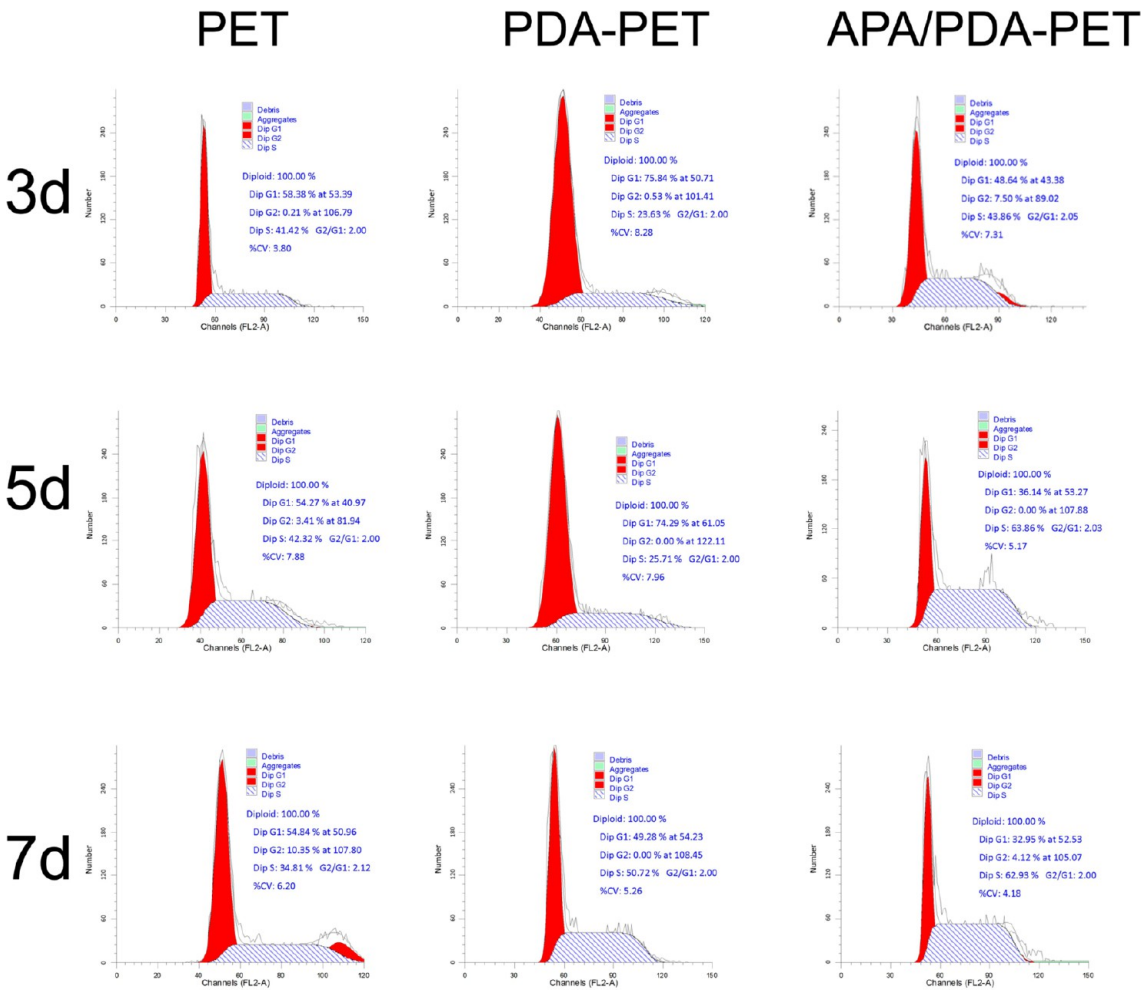

Figure 5. Cell cycle analysis. PET, polyethylene terephthalate; PDA, polydopamine; APA, apatite.

The morphological grading results for the interface tissue at the graft−bone interface are shown in Table 3. In the APA/PDA−PET group, a transitional connection zone composed of fibrocartilage was observed at the graft−bone interface 12 weeks after surgery (Figure 8B,C). In the PET and PDA−PET groups, no obvious fibrocartilage transition zone was observed at the graft−bone interface.

4. DISCUSSION

In this study, a uniform APA/PDA hybrid nanolayer was successfully prepared on the surface of PET artificial ligament grafts using a mussel-inspired biomimetic method. Dopamine can polymerize and form self-assembled polydopamine films that can uniformly adhere to the surface of different types of materials.[14,19] The self-assembled polydopamine film provides nucleation sites, such as OH^- and NH^{2-}, for CaP apatite mineralization.[17] In this study, a self-assembled apatite/polydopamine hybrid layer forms on the surface of the PET grafts. This approach is a facile but useful method for modifying PET grafts with significantly improved bioactivity, where Ca, P ions and dopamine-containing SBF can be easily prepared followed by the formation of a self-assembled polydopamine film simultaneously occurring with the mineralization of nanosized CaP apatite particles to form an APA/PDA hybrid layer on the surface of PET. In comparison to conventional modification methods for PET, such as the physical deposition technique,[13,20] the CaP apatite/PDA hybrid coating can be efficiently used for modifying the surface of PET with a uniform nanostructure using this mussel-inspired biomimetic method. Because of the APA/PDA hybrid layer on the surface of PET, the prepared APA/PDA−PET grafts exhibited distinct *in vitro* and *in vivo* bioactivity for ligament reconstruction, as shown in Figure 1.

One of the important results in this study is that the prepared APA/PDA−PET grafts significantly stimulated the proliferation and osteogenic/angiogenic differentiation of BMSCs, which was based on the proliferation and expression levels of the osteogenesis/angiogenesis-related genes (e.g., ALP, OPN, Runx2 and VEGF) of BMSCs being substantially enhanced by the APA/PDA−PET grafts. Correspondingly, the expression of the osteogenesis/angiogenesis-related proteins (e.g., BMP-2, HIF-1α and VEGF) was also enhanced by the APA/PDA−PET grafts. ALP is known as a key marker for early osteogenesis, and OPN and Runx2 are both important markers for osteogenic differentiation of BMSCs,[21] indicating that the APA/PDA hybrid layer possessed the ability to stimulate *in vitro* osteogenesis of BMSCs. In addition, graft−bone healing is not only associated with osteogenesis but also depends on angiogenesis at the graft−bone interface.[20,22] Angiogenesis is directed by a variety of growth factors in a complex multistep process, and VEGF has been identified as a key regulator. VEGF activates endothelial cells in the surrounding tissue by stimulating their migration and proliferation as well as the formation of blood vessel structures.[23] Ingrowth of new blood vessels is an essential step in the process

DOI: 10.1021/acsami.5b05109
ACS Appl. Mater. Interfaces 2015, 7, 14708−14719

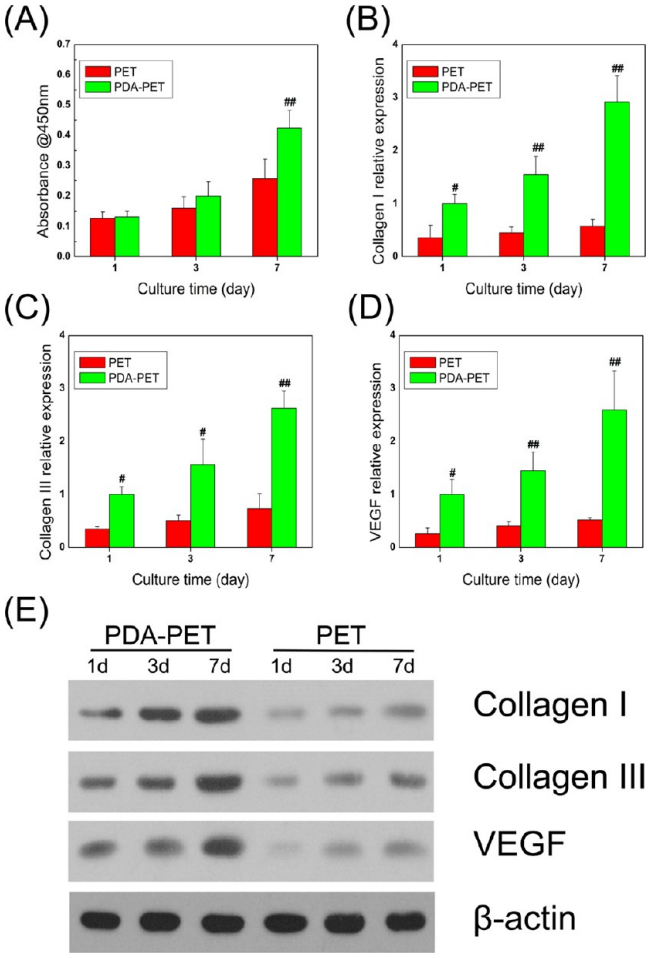

Figure 6. (A) Proliferation of ACL cells on PET and PDA–PET grafts. (B) Real-time PCR analysis of Collagen I gene levels on PET and PDA–PET grafts. (C) Real-time PCR analysis of Collagen III gene levels on PET and PDA–PET grafts. (D) Real-time PCR analysis of VEGF gene levels on PET and PDA–PET grafts. (E) Western blotting analysis for collagen I, Collagen III and VEGF. ## ($p < 0.01$) or # ($p < 0.05$) indicate a significant difference between PDA–PET and PET group. PET, polyethylene terephthalate; PDA, polydopamine.

of graft remodeling at the graft–bone interface, and angiogenesis is also essential to osteogenesis.[22] During the bone healing process, VEGF interacts synergistically with BMP-2 to promote bone formation and bone healing via modulation of angiogenesis.[24,25] HIF-1α is involved in the activation of VEGF and initiates the expression of a number of genes associated with tissue regeneration and skeletal tissue development that are activated in fracture repair.[26] In this study, an angiogenesis-related gene (VEGF) and proteins (HIF-1α and VEGF) were significantly enhanced by the APA/PDA–PET grafts, indicating that the APA/PDA hybrid layer was able to stimulate *in vitro* angiogenesis of BMSCs.

Several important factors may contribute to the stimulatory effect of the APA/PDA–PET grafts on the proliferation and osteogenesis/angiogenesis of BMSCs. First, the improvement in the cell proliferation may be directly related to the improvement in the bioactive functional groups (e.g., OH and NH_2) from PDA.[19] Second, the mineralization of nanosized CaP apatite on the surface of the grafts may assist cell-adhesive ECM protein (e.g., fibronectin) adsorption and further contributes to the proliferation and differentiation of BMSCs.[17] Third, the improvement in the surface hydrophilicity of PET may contribute to the promotion of cell activity.[21] PDA can substantially enhance the hydrophilicity and biocompatibility of biomaterials.[27−31] After mineralization, the APA/PDA–PET grafts possessed a significantly lower contact angle than that of pure PET grafts, indicating that the APA/PDA nanolayer significantly improved the surface hydrophilicity of PET grafts. Therefore, both PDA and the nano CaP apatite phase in the APA/PDA–PET grafts have a synergistic effect on stimulating the proliferation and osteogenic/angiogenic differentiation of BMSCs.

To explore further the mechanism of the stimulatory effect of the APA/PDA–PET grafts on the osteogenic/angiogenic differentiation of BMSCs, the PKC signaling pathway was blocked. The inhibition of the PKC activity reduced the P-ERK1/2 production and further inhibited BMP-2, OPN and OCN expression of BMSCs on the APA/PDA–PET grafts. Previous results indicated that extracellular Ca and P ions played an important role in aiding osteoblastic differentiation,[32,33] and Ca ions were required for PKC/p-ERK1/2 phosphorylation and regulation of mineralization-associated genes in osteoblasts.[34] P-ERK1/2 is an important signaling pathway that is related to osteogenic differentiation. Therefore, our results suggest that the formed Ca, P-containing nanolayer on the APA/PDA–PET grafts may play a key role in activating the PKC/p-ERK1/2 pathway of BMSCs and further stimulating their osteogenic differentiation.

The other important innovation of the current study is that the prepared APA/PDA–PET grafts significantly stimulated *in vivo* osseointegration. In our study, the histological and Micro-CT results correlated with the improved biomechanical properties (i.e., pull-out load capacity). Bone formation is one of primary factors involved in the graft osseointegration process after *in vivo* implantation.[20] As previously mentioned, the APA/PDA–PET grafts have dual functions to stimulate *in vitro* osteogenesis/angiogenesis of BMSCs, which further enhances new bone growth into the grafts. In this study, the maximal pull-out load of the APA/PDA–PET group was significantly higher than that of the pure PET group without coatings 12 weeks after surgery. The pull-out load capacity suggests the biomechanical stability of the grafts in the bone tunnel.[35] In addition, no significant difference in the maximal pull-out load was detected between the PDA–PET and PET groups at week 12, and the maximal pull-out load of the APA/PDA–PET group was significantly higher than that of the PDA–PET group. These results indicate that the formed APA/PDA hybrid nanolayer on the grafts may have a synergistic effect on the improvement of their biomechanical strength and osseointegration.

In addition, the APA/PDA–PET grafts induced the formation of biomimetic tissue structure of the ligaments with regenerated fibrocartilage characterizing a transitional zone from graft to bone. This type of biomimetic tissue structure of the ligament cannot be regenerated by conventional methods. Previously, various types of hydrophilic and/or bioactive materials (e.g., polymers and bioceramics, such as chitosan–hyaluronic acid (CH) composite, polystyrene sodium sulfonate (PolyNASS), hydroxyapatite (HAp) and bioactive glass) have been applied to modify the surface of PET grafts to improve their surface bioactivity.[13,20,36−40] These coatings improved the graft-to-bone contact by increasing new bone formation and decreasing fibrous scar tissue at the graft–bone interface. However, these methods cannot induce a biomimetic fibrocartilage transitional zone from the graft to the bone. The biomimetic fibrocartilage transitional

DOI: 10.1021/acsami.5b05109
ACS Appl. Mater. Interfaces 2015, 7, 14708−14719

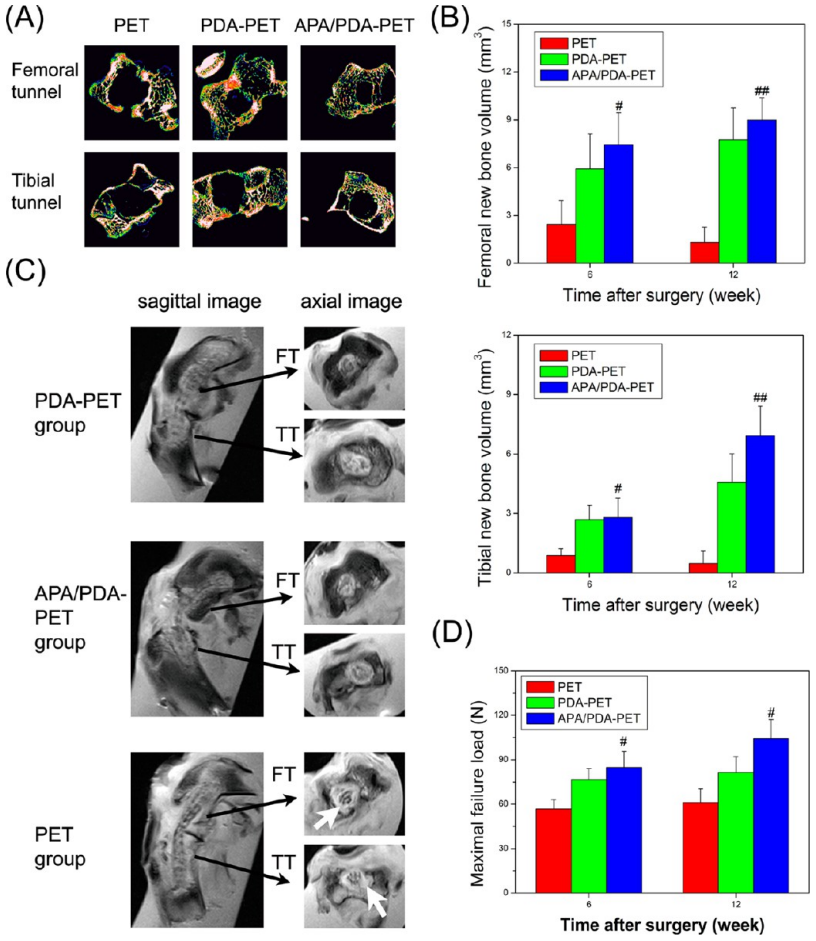

Figure 7. (A) *In vivo* bone formation at the graft−bone interface after implanted for 12 weeks as assessed by micro-CT, indicating the size of bone tunnel defects tends to become small after implanted with APA/PDA−PET grafts. (B) Quantitative results of new bone formation in the middle portion of the femoral and tibial bone tunnel, indicating that APA/PDA−PET grafts induce more mineralized tissue formation than PET grafts. (C) Magnetic resonance images of the ACL-reconstructed knees show the graft−bone interface among the PET, PDA−PET and APA/PDA−PET groups after implanted for 12 weeks. The graft−bone interface of PET group revealed the highest signal (white arrow), indicating fibrous scar tissue at the graft−bone interface for PET, whereas APA/PDA−PET grafts show a low signal, indicating that APA/PDA−PET grafts induce mineralized tissue formation. (D) Biomechanical results of three grafts at each time point after surgery. The maximal pull-out load of APA/PDA−PET group was significantly higher than that of PET group at 12 weeks (indicated by #). ## ($p < 0.01$) or # ($p < 0.05$) indicate a significant difference between the PET group and the APA/PDA−PET group. FT, femoral tunnel; TT, tibial tunnel.

structure may effectively eliminate high levels of stress at the graft−bone interface and afford effective transfer of mechanical loads between soft tissue and hard tissue.[41] However, in contrast to the natural tendon−bone insertion site, direct graft−bone contact cannot effectively diminish the stress concentration at the interface.

Currently, the detailed mechanism that governs the formation of the fibrocartilage interface remains unclear. In this study, the synergistic effect of the formed APA/PDA hybrid nanolayer may contribute to the formation of fibrocartilage at the graft−bone interface. With bioactive functional groups (e.g., OH, NH_2) and improved hydrophilicity, PDA may promote the aggregation of mesenchymal cells and facilitate multidirectional differentiation of mesenchymal cells, which might stimulate the formation of a collagen fiber matrix.[42] In addition, CaP apatite mineralization could accelerate the formation of a fibrocartilage tissue layer and improve collagen organization at the healing tendon−bone insertion site,[11,12,43] which may be related to the multiple roles of Ca^{2+} mediated cartilage-like tissue production.[44]

5. CONCLUSIONS

In this study, a uniform APA/PDA hybrid nanolayer on the surface of PET artificial ligaments was successfully prepared using a mussel-inspired biomimetic method. The prepared APA/PDA hybrid nanolayer on PET significantly stimulated the proliferation and osteogenic/angiogenic differentiation of BMSCs by activating the PKC/p-ERK1/2 signaling pathway. In addition, the *in vivo* study in a rabbit ACL reconstruction model demonstrated that the APA/PDA−PET grafts resulted in significantly improved osseointegration by promoting new bone formation at the graft−bone interface and enhancing the biomechanical strength. In particular, the APA/PDA−PET grafts induced the formation of a biomimetic tissue structure of the ligaments due to the regenerated fibrocartilage transitional zone from the graft to the bone. Both the *in vitro* and *in vivo* results suggest that mussel-inspired grafts can be used for functional ligament reconstruction via a synergistic effect of polydopamine and apatite.

DOI: 10.1021/acsami.5b05109
ACS Appl. Mater. Interfaces 2015, 7, 14708−14719

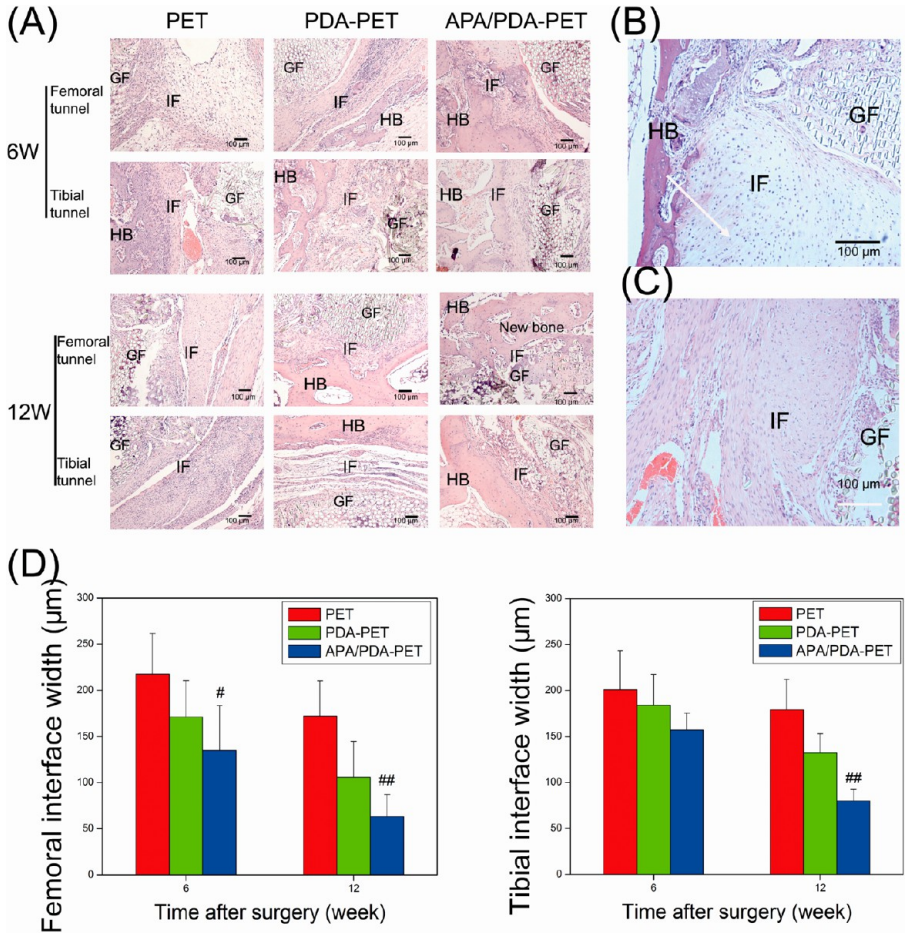

Figure 8. (A) Hematoxylin−eosin (HE) staining results for the graft−bone interface at PET, PDA−PET and APA/PDA−PET groups after implanted for 6 and 12 weeks. Bar = 100 μm. APA/PDA−PET grafts induce more distinct new bone formation at the interface than other two groups. (B) HE staining of a regenerated fibrocartilage transitional zone from graft to bone in APA/PDA−PET group (arrow pointing to fibrocartilage). (C) Masson trichrome staining of a regenerated fibrocartilage transitional zone from graft to bone in APA/PDA−PET group (arrow pointing to fibrocartilage). (D) Quantitative analysis of graft−bone interface width (n = 5). The interface width decreased distinctively after implanted with APA/PDA−PET grafts, indicating that APA/PDA−PET grafts stimulating osseointegration. ## ($p < 0.01$) or # ($p < 0.05$) indicate a significant difference between APA/PDA−PET and PET groups. Mussel-inspired APA/PDA−PET grafts significantly improved *in vivo* osseointegration as compared to PET and PDA−PET grafts. HB, host bone; IF, interface; G, graft.

Table 3. Yamakado Interface Morphological Grade

	6 weeks			12 weeks		
	PET	PDA−PET	APA/PDA−PET	PET	PDA−PET	APA/PDA−PET
separation	1/10	0/10	0/10	1/10	0/10	0/10
interface	2/10	3/10	2/10	4/10	2/10	2/10
indirect type	7/10	7/10	8/10	5/10	8/10	6/10
direct type	0/10	0/10	0/10	0/10	0/10	2/10

AUTHOR INFORMATION

Corresponding Authors

*Prof. Dr. Chengtie Wu. E-mail: chengtiewu@mail.sic.ac.cn. Tel: +86-21-52422804. Fax: +86-21-52413903.

*Prof. Dr. Shiyi Chen. E-mail: cshiyi@163.com. Tel: +86-21-52888255. Fax: +86-21-62496020.

Notes

The authors declare no competing financial interest.

ACKNOWLEDGMENTS

This project was subsidized by the Recruitment Program of Global Young Talent, China (Dr. Wu), the National High Technology Research and Development Program of China (863 Program, SS2015AA020302), Natural Science Foundation of China (81201202, 81401812), Program of Shanghai Outstanding Academic Leaders (15XD1503900), and innovative project of SIC, CAS.

REFERENCES

(1) Marrale, J.; Morrissey, M. C.; Haddad, F. S. A literature review of autograft and allograft anterior cruciate ligament reconstruction. *Knee Surg Sports Traumatol Arthrosc* **2007**, *15* (6), 690−704.

(2) Spindler, K. P.; Wright, R. W. Clinical practice. Anterior cruciate ligament tear. *N. Engl. J. Med.* **2008**, *359* (20), 2135−42.

DOI: 10.1021/acsami.5b05109
ACS Appl. Mater. Interfaces 2015, 7, 14708−14719

(3) Liu, Z. T.; Zhang, X. L.; Jiang, Y.; Zeng, B. F. Four-strand hamstring tendon autograft versus LARS artificial ligament for anterior cruciate ligament reconstruction. *Int. Orthop* **2010**, *34* (1), 45−9.
(4) Parchi, P. D.; Gianluca, C.; Dolfi, L.; Baluganti, A.; Nicola, P.; Chiellini, F.; Lisanti, M. Anterior cruciate ligament reconstruction with LARS artificial ligament results at a mean follow-up of eight years. *Int. Orthop* **2013**, *37* (8), 1567−74.
(5) Shen, G.; Xu, Y.; Dong, Q.; Zhou, H.; Yu, C. Arthroscopic posterior cruciate ligament reconstruction using LARS artificial ligament: a retrospective study. *J. Surg. Res.* **2012**, *173* (1), 75−82.
(6) Hamido, F.; Misfer, A. K.; Al Harran, H.; Khadrawe, T. A.; Soliman, A.; Talaat, A.; Awad, A.; Khairat, S. The use of the LARS artificial ligament to augment a short or undersized ACL hamstrings tendon graft. *Knee* **2011**, *18* (6), 373−8.
(7) Ranger, P.; Renaud, A.; Phan, P.; Dahan, P.; De Oliveira, E., Jr.; Delisle, J. Evaluation of reconstructive surgery using artificial ligaments in 71 acute knee dislocations. *Int. Orthop* **2011**, *35* (10), 1477−82.
(8) Gao, K.; Chen, S.; Wang, L.; Zhang, W.; Kang, Y.; Dong, Q.; Zhou, H.; Li, L. Anterior cruciate ligament reconstruction with LARS artificial ligament: a multicenter study with 3- to 5-year follow-up. *Arthroscopy* **2010**, *26* (4), 515−23.
(9) Viateau, V.; Manassero, M.; Anagnostou, F.; Guerard, S.; Mitton, D.; Migonney, V. Biological and biomechanical evaluation of the ligament advanced reinforcement system (LARS AC) in a sheep model of anterior cruciate ligament replacement: a 3-month and 12-month study. *Arthroscopy* **2013**, *29* (6), 1079−88.
(10) Shen, H.; Qiao, G.; Cao, H.; Jiang, Y. An histological study of the influence of osteoinductive calcium phosphate ceramics on tendon healing pattern in a bone tunnel with suspensory fixation. *Int. Orthop* **2010**, *34* (6), 917−24.
(11) Mutsuzaki, H.; Sakane, M. Calcium phosphate-hybridized tendon graft to enhance tendon-bone healing two years after ACL reconstruction in goats. *Sports Med. Arthrosc Rehabil Ther Technol.* **2011**, *3* (1), 31.
(12) Zhao, S.; Peng, L.; Xie, G.; Li, D.; Zhao, J.; Ning, C. Effect of the Interposition of Calcium Phosphate Materials on Tendon-Bone Healing During Repair of Chronic Rotator Cuff Tear. *Am. J. Sports Med.* **2014**, *42* (8), 1920−1929.
(13) Li, H.; Ge, Y.; Wu, Y.; Jiang, J.; Gao, K.; Zhang, P.; Wu, L.; Chen, S. Hydroxyapatite coating enhances polyethylene terephthalate artificial ligament graft osseointegration in the bone tunnel. *Int. Orthop* **2011**, *35* (10), 1561−7.
(14) Lee, H.; Dellatore, S. M.; Miller, W. M.; Messersmith, P. B. Mussel-inspired surface chemistry for multifunctional coatings. *Science* **2007**, *318* (5849), 426−30.
(15) Wu, C. T.; Fan, W.; Chang, J.; Xiao, Y. Mussel-inspired porous SiO2 scaffolds with improved mineralization and cytocompatibility for drug delivery and bone tissue engineering. *J. Mater. Chem.* **2011**, *21*, 18300−18307.
(16) Gajjeraman, S.; He, G.; Narayanan, K.; George, A. Biological assemblies provide novel templates for the synthesis of hierarchical structures and facilitate cell adhesion. *Adv. Funct. Mater.* **2008**, *18* (24), 3972−3980.
(17) Wu, C.; Han, P.; Liu, X.; Xu, M.; Tian, T.; Chang, J.; Xiao, Y. Mussel-inspired bioceramics with self-assembled Ca-P/polydopamine composite nanolayer: preparation, formation mechanism, improved cellular bioactivity and osteogenic differentiation of bone marrow stromal cells. *Acta Biomater.* **2014**, *10* (1), 428−38.
(18) Xu, M. C.; Zhang, Y. F.; Zhai, D.; Chang, J.; Wu, C. T. Mussel-inspired bioactive ceramics with improved bioactivity, cell proliferation, differentiation and bone-related gene expression of MC3T3 cells. *Biomater. Sci.* **2013**, *1* (9), 933−941.
(19) Ryu, J.; Ku, S. H.; Lee, H.; Park, C. B. Mussel-inspired polydopamine coating as a universal route to hydroxyapatite crystallization. *Adv. Funct. Mater.* **2010**, *20* (13), 2132−9.
(20) Li, H.; Chen, S.; Wu, Y.; Jiang, J.; Ge, Y.; Gao, K.; Zhang, P.; Wu, L. Enhancement of the osseointegration of a polyethylene terephthalate artificial ligament graft in a bone tunnel using 58S bioglass. *Int. Orthop* **2012**, *36* (1), 191−7.
(21) Wu, C.; Zhou, Y.; Xu, M.; Han, P.; Chen, L.; Chang, J.; Xiao, Y. Copper-containing mesoporous bioactive glass scaffolds with multifunctional properties of angiogenesis capacity, osteostimulation and antibacterial activity. *Biomaterials* **2013**, *34* (2), 422−33.
(22) Sasaki, K.; Kuroda, R.; Ishida, K.; Kubo, S.; Matsumoto, T.; Mifune, Y.; Kinoshita, K.; Tei, K.; Akisue, T.; Tabata, Y.; Kurosaka, M. Enhancement of tendon-bone osteointegration of anterior cruciate ligament graft using granulocyte colony-stimulating factor. *Am. J. Sports Med.* **2008**, *36* (8), 1519−27.
(23) Wu, C.; Zhou, Y.; Fan, W.; Han, P.; Chang, J.; Yuen, J.; Zhang, M.; Xiao, Y. Hypoxia-mimicking mesoporous bioactive glass scaffolds with controllable cobalt ion release for bone tissue engineering. *Biomaterials* **2012**, *33* (7), 2076−85.
(24) Peng, H.; Usas, A.; Olshanski, A.; Ho, A. M.; Gearhart, B.; Cooper, G. M.; Huard, J. VEGF improves, whereas sFlt1 inhibits, BMP2-induced bone formation and bone healing through modulation of angiogenesis. *J. Bone Miner. Res.* **2005**, *20* (11), 2017−27.
(25) Yu, X.; Khalil, A.; Dang, P. N.; Alsberg, E.; Murphy, W. L. Multilayered Inorganic Microparticles for Tunable Dual Growth Factor Delivery. *Adv. Funct. Mater.* **2014**, *24* (20), 3082−3093.
(26) Hu, X.; Yu, S. P.; Fraser, J. L.; Lu, Z.; Ogle, M. E.; Wang, J. A.; Wei, L. Transplantation of hypoxia-preconditioned mesenchymal stem cells improves infarcted heart function via enhanced survival of implanted cells and angiogenesis. *J. Thorac. Cardiovasc. Surg.* **2008**, *135* (4), 799−808.
(27) Lynge, M. E.; van der Westen, R.; Postma, A.; Stadler, B. Polydopamine–a nature-inspired polymer coating for biomedical science. *Nanoscale* **2011**, *3* (12), 4916−28.
(28) Jiang, J.; Zhu, L.; Zhu, B.; Xu, Y. Surface characteristics of a self-polymerized dopamine coating deposited on hydrophobic polymer films. *Langmuir* **2011**, *27* (23), 14180−7.
(29) Mangindaan, D.; Yared, I.; Kurniawan, H.; Sheu, J. R.; Wang, M. J. Modulation of biocompatibility on poly(vinylidene fluoride) and polysulfone by oxygen plasma treatment and dopamine coating. *J. Biomed. Mater. Res., Part A* **2012**, *100* (11), 3177−88.
(30) Wei, Q.; Li, B.; Yi, N.; Su, B.; Yin, Z.; Zhang, F.; Li, J.; Zhao, C. Improving the blood compatibility of material surfaces via biomolecule-immobilized mussel-inspired coatings. *J. Biomed. Mater. Res., Part A* **2011**, *96* (1), 38−45.
(31) Zhu, L. P.; Jiang, J. H.; Zhu, B. K.; Xu, Y. Y. Immobilization of bovine serum albumin onto porous polyethylene membranes using strongly attached polydopamine as a spacer. *Colloids Surf., B* **2011**, *86* (1), 111−8.
(32) Hu, F.; Pan, L.; Zhang, K.; Xing, F.; Wang, X.; Lee, I.; Zhang, X.; Xu, J. Elevation of extracellular Ca2+ induces store-operated calcium entry via calcium-sensing receptors: a pathway contributes to the proliferation of osteoblasts. *PLoS One* **2014**, *9* (9), e107217.
(33) Shih, Y. R.; Hwang, Y.; Phadke, A.; Kang, H.; Hwang, N. S.; Caro, E. J.; Nguyen, S.; Siu, M.; Theodorakis, E. A.; Gianneschi, N. C.; Vecchio, K. S.; Chien, S.; Lee, O. K.; Varghese, S. Calcium phosphate-bearing matrices induce osteogenic differentiation of stem cells through adenosine signaling. *Proc. Natl. Acad. Sci. U. S. A.* **2014**, *111* (3), 990−5.
(34) Samavedi, S.; Whittington, A. R.; Goldstein, A. S. Calcium phosphate ceramics in bone tissue engineering: a review of properties and their influence on cell behavior. *Acta Biomater.* **2013**, *9* (9), 8037−45.
(35) Li, H.; Wu, C.; Chang, J.; Ge, Y.; Chen, S. Functional Polyethylene Terephthalate with Nanometer-Sized Bioactive Glass Coatings Stimulating In Vitro and In Vivo Osseointegration for Anterior Cruciate Ligament Reconstruction. *Adv. Mater. Interfaces* **2014**, *1*, 1400027.
(36) Gustafsson, Y.; Haag, J.; Jungebluth, P.; Lundin, V.; Lim, M. L.; Baiguera, S.; Ajalloueian, F.; Del Gaudio, C.; Bianco, A.; Moll, G.; Sjoqvist, S.; Lemon, G.; Teixeira, A. I.; Macchiarini, P. Viability and proliferation of rat MSCs on adhesion protein-modified PET and PU scaffolds. *Biomaterials* **2012**, *33* (32), 8094−103.
(37) Li, H.; Ge, Y.; Zhang, P.; Wu, L.; Chen, S. The effect of layer-by-layer chitosan-hyaluronic acid coating on graft-to-bone healing of a poly(ethylene terephthalate) artificial ligament. *J. Biomater. Sci., Polym. Ed.* **2012**, *23* (1−4), 425−38.

DOI: 10.1021/acsami.5b05109
ACS Appl. Mater. Interfaces 2015, 7, 14708−14719

(38) Cho, S.; Li, H.; Chen, C.; Jiang, J.; Tao, H.; Chen, S. Cationised gelatin and hyaluronic acid coating enhances polyethylene terephthalate artificial ligament graft osseointegration in porcine bone tunnels. *Int. Orthop* **2013**, *37* (3), 507−13.
(39) Vaquette, C.; Viateau, V.; Guerard, S.; Anagnostou, F.; Manassero, M.; Castner, D. G.; Migonney, V. The effect of polystyrene sodium sulfonate grafting on polyethylene terephthalate artificial ligaments on in vitro mineralisation and in vivo bone tissue integration. *Biomaterials* **2013**, *34* (29), 7048−63.
(40) Yang, J.; Jiang, J.; Li, Y.; Li, H.; Jing, Y.; Wu, P.; Yu, D.; Chen, S. A new strategy to enhance artificial ligament graft osseointegration in the bone tunnel using hydroxypropylcellulose. *Int. Orthop* **2013**, *37* (3), 515−21.
(41) Li, X.; Xie, J.; Lipner, J.; Yuan, X.; Thomopoulos, S.; Xia, Y. Nanofiber scaffolds with gradations in mineral content for mimicking the tendon-to-bone insertion site. *Nano Lett.* **2009**, *9* (7), 2763−8.
(42) Tsai, W. B.; Chen, W. T.; Chien, H. W.; Kuo, W. H.; Wang, M. J. Poly(dopamine) coating of scaffolds for articular cartilage tissue engineering. *Acta Biomater.* **2011**, *7* (12), 4187−94.
(43) Kovacevic, D.; Fox, A. J.; Bedi, A.; Ying, L.; Deng, X. H.; Warren, R. F.; Rodeo, S. A. Calcium-phosphate matrix with or without TGF-beta3 improves tendon-bone healing after rotator cuff repair. *Am. J. Sports Med.* **2011**, *39* (4), 811−9.
(44) Farnsworth, N. L.; Mead, B. E.; Antunez, L. R.; Palmer, A. E.; Bryant, S. J. Ionic osmolytes and intracellular calcium regulate tissue production in chondrocytes cultured in a 3D charged hydrogel. *Matrix Biol.* **2014**, *40*, 17−26.

DOI: 10.1021/acsami.5b05109
ACS Appl. Mater. Interfaces 2015, 7, 14708−14719